NEUTRON CHARGE DISTRIBUTION AND CHARGE DENSITY DISTRIBUTIONS IN LEAD ISOTOPES

S. Haddad and S. Suleiman

Physics Department, Atomic Energy Commission of Syria
P.O.BOX 6091, Damascus, Syria

An analytical fit to the experimental data on the mean square charge radius and to QCD-calculations of the neutron charge distribution is given and used to recognize the neutron charge distribution when calculating the charge density distribution in a finite nucleus. Relativistic Thomas–Fermi calculations of lead isotopes are performed and the effect of the neutron charge distribution on charge density distributions and rms charge radii of lead isotopes is discussed.

1. Introduction

The determination of the mean square charge radius of the neutron has found a great interest, since it is related to the scattering length describing neutron-electron scattering [1]. Precise knowledge of the charge distribution within the neutron may give important clues about the strong forces binding quarks together [2].

New measurements of the charge radius of the neutron show that the neutron has a mean square charge radius of $\langle r_n^2 \rangle = -0.113 \pm 0.007$ fm^2, where the negative sign is attributed to the negative π-meson cloud [1]. This value has been expected to be reliable, since a modern technology for detector and data acquisition systems has been applied in the experiment described in Ref. [1]. Furthermore, measurements are done using thorogenic lead and a part of this work concentrates on the study of the effect of the neutron charge distribution on the Pb isotope shifts.

Quantum chromodynamics (QCD) calculations indicate that the neutron has a positive core and a negative outer region [2]. The charge density distribution in a finite nucleus is usually calculated by folding the proton

density with a Gaussian representing the charge distribution in the proton [3], ignoring the charge distribution in the neutron or taking it into account as a small correction to the charge rms radius [4].

In this work an analytical fit to the experimental data on the mean square charge radius of the neutron and to QCD-calculations of the neutron charge distribution is given, and used to recognize the neutron charge distribution when calculating the charge density distribution in a finite nucleus. Relativistic Thomas–Fermi calculations [5,6] of lead isotopes are performed first with the neutron charge distribution ignored and then with the neutron charge distribution recognized when calculating the charge density distribution in a Pb-isotope. The study of the charge density distributions in lead isotopes has gained considerable interest in recent years because of the kink observed in the isotope shifts of Pb nuclei [7,8].

The effect of the neutron charge distribution on the charge density distributions in lead isotopes is discussed and the correction of the isotope shifts is compared with experiment and with the formula given in Ref. [4].

2. Charge distribution in a finite nucleus

The charge density is usually calculated by folding the proton density with a Gaussian representing the charge distribution of the proton [3]:

$$\rho_{\rm ch}(r) = \int d^3r' \rho_p(r') g(|\vec{r} - \vec{r}\,'|) \,, \tag{1}$$

with:

$$g(r) = \left(r_0\sqrt{\pi}\right)^{-3} {\rm e}^{-(r/r_0)^2} \,, \tag{2}$$

with $r_0 = \sqrt{2/3}\langle r_p\rangle_{\rm rms}$, the rms charge radius of the proton being $\langle r_p\rangle_{\rm rms} = 0.8$ fm.

The charge distribution of the neutron is recognized when calculating the charge density in a finite nucleus by using:

$$\rho_{\rm ch}(r) = \int d^3r' \left[\rho_p(r') g_p(|\vec{r} - \vec{r}\,'|) + \rho_n(r') g_n(|\vec{r} - \vec{r}\,'|)\right] \tag{3}$$

instead of Eq. (1). g_p is still given by Eq. (2) and for $g_n(r)$ we use the following form:

$$g_n(r) = -\frac{2}{3} \frac{\langle r_n^2\rangle}{r_1^2(r_1\sqrt{\pi})^3} \left(\frac{r}{r_1}\right)^2 \left[1 - \frac{2}{5}\left(\frac{r}{r_1}\right)^2\right] {\rm e}^{-(r/r_1)^2} \,. \tag{4}$$

This equation represents a 3-parametric fit to the charge density distribution within the neutron. The factor 2/5 in the brackets guarantees that:

$$\int d^3r \; g_n(r) = 0 \,, \tag{5}$$

i.e., the total charge of the neutron is zero, and the constant is necessary to reproduce $\langle r_n^2 \rangle$ as the rms value of $g_n(r)$, *i.e.*:

$$\int d^3r \; r^2 \; g_n(r) = \langle r_n^2 \rangle = -0.113 \text{ fm}^2 \,. \tag{6}$$

The third parameter r_1 is a scaling parameter, which is necessary to define a dimensionless quantity (r/r_1) in the Gaussian exponent. The results of QCD-calculations of the charge density distribution inside the neutron [2] are best reproduced by choosing:

$$r_1 = \sqrt{\frac{2}{5}} \cdot 0.71 \text{ fm} \,. \tag{7}$$

Fig. 1 illustrates $g_n(r)$. A remark concerning the use of Gaussian parametrizations of the proton and neutron charge distributions should be added at this stage. There are other common ways to include the effects of the proton and the neutron charge distributions, like constructing the charge distributions corresponding to experimentally determined form factors of the proton and neutron, and convoluting these distributions with the point proton and neutron wave functions, respectively. This has been done, for instance, in Ref. [9]. The comparison between our results and those of Ref. [9] indicates that charge radii are not particularly sensitive to such details.
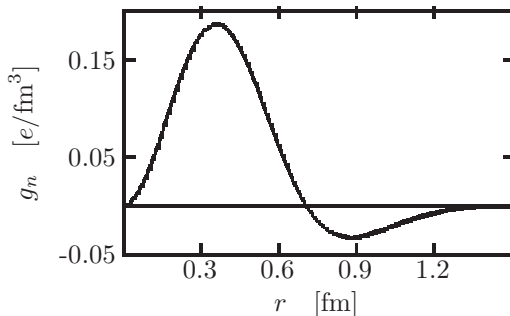

Fig. 1. Analytical fit to the distribution of electric charge within the neutron $g_n(r)$.

3. Charge distribution in lead isotopes

Lead isotopes are calculated utilizing the relativistic Thomas–Fermi approximation with the parameter set H1 of Ref. [5], which is given in Table I, together with the saturation properties of nuclear matter it produces.

It has been shown in Ref. [5] that the relativistic Thomas-Fermi approximation poorly reproduces the experimental charge density distribution of

Model parameters and nuclear matter saturation properties. Parameter set H1 is taken from Ref. [5]. The nucleon mass is $m_N = 939$ MeV. ρ_0 is the saturation density, k_F the saturation Fermi wave number, a_v the saturation energy per particle (volume energy), and K the incompressibility.

Meson	σ	ω	ρ
Mass [MeV]	550	783	770
$g^2/4\pi$	9.7668	15.167	0.55

$\rho_0[\text{fm}^{-3}]$	$k_F[\text{fm}^{-1}]$	a_v [MeV]	K [MeV]
0.148	1.30	-15.75	545

^{208}Pb, but with the parameter set H1 it produces an accurate value for the rms charge radius of ^{208}Pb. More sophisticated approximations than the relativistic Thomas–Fermi approximation are expected to produce better results for the proton and neutron density distributions, but we expect the effect of including the charge density distribution within the neutron via Eq. (3) to be almost the same in the simple Thomas–Fermi approximation as in more sophisticated approximations.

Charge density distributions are calculated in two different ways. In the first (noted by TF1) relation (1) is used, and in the second (TF2) relation (3). The difference between TF1 and TF2 is clearly given by the second term on the right-hand side of Eq. (3), which represents the effect of taking the charge distribution within the neutron into account.

Figure 2 shows the charge density distribution in ^{208}Pb, and figure 3 shows the difference $\Delta\rho_{\text{ch}}$ between the TF2 and TF1 results for the charge density distribution in ^{208}Pb, *i.e.*, the second term on the right-hand side of Eq. (3).

One result of using Eq. (3) is that $\rho_{\text{ch}}(r)$ might get negative at the surface region of nuclei with thick neutron skin. This is seen in figure 3 and the neutron skin thickness of lead isotopes [11, 12]:

$$t = r_n - r_p \,, \qquad (8)$$

where r_n and r_p are the rms radii of the neutron and proton density distributions, respectively, are given in Table II. This negative charge is the result of the form of $g_n(r)$ shown in Fig. 1 and can be removed only by assuming that the neutron charge distribution changes due to polarisation effects in a finite nucleus, especially for neutrons in the neutron skin region. The range of the nuclear force is short, and the neighboring nucleons which

TABLE II

The charge radii, neutron skin thickness, and binding energies per particle obtained for *Pb*-isotopes using the parameter set H1 given in Table I. Experimental values are taken from Refs [8, 13].

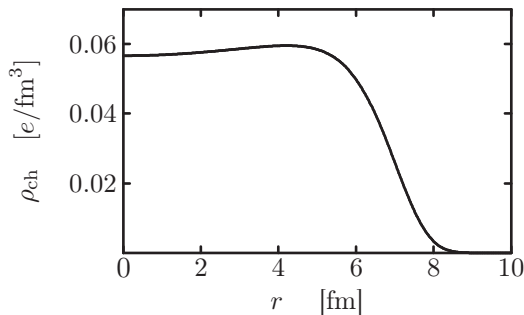| A	r_{ch} [fm]			t [fm]		B/A [MeV]	
	TF1	TF2	Exp.	TF	Exp.	TF	Exp.
200	5.470	5.455	5.464	0.120		−6.780	−7.882
202	5.482	5.467	5.473	0.131		−6.792	−7.882
204	5.494	5.479	5.483	0.142		−6.802	−7.880
206	5.506	5.490	5.492	0.153	0.181	−6.810	−7.875
208	5.518	5.502	5.503	0.164	0.197	−6.816	−7.868
210	5.530	5.514	5.522	0.175		−6.816	−7.836
212	5.542	5.526	5.540	0.186		−6.819	−7.804
214	5.554	5.538	5.558	0.196		−6.818	−7.772

Fig. 2. Charge density distribution in ^{208}Pb. The differences between the TF1 and TF2 distributions are too small to be seen in this figure, they are shown in Fig. 3.

can alter the internal structure of the interacting nucleons must be close. For neutrons in the neutron skin region such neighboring nucleons are more abundant in the direction pointing to the center of the nucleus.

Table II shows the results for the rms charge radii of Pb-isotopes, and, for completeness, the results for the binding energies, and compare this results with experimental data. The effect of recognizing the neutron charge distribution on the rms charge radii of lead isotopes is very well reproduced by:

$$\left(r_{ch}^2\right)_{TF2} = \left(r_{ch}^2\right)_{TF1} + \frac{N}{Z}\langle r_n^2\rangle. \tag{9}$$

The formula given in Ref. [4] for the effect of recognizing the charge distribution within the neutron on the Pb isotope shifts:

$$\Delta r_{ch}^2(A) = r_{ch}^2\left(^A\text{Pb}\right) - r_{ch}^2\left(^{208}\text{Pb}\right) \tag{10}$$
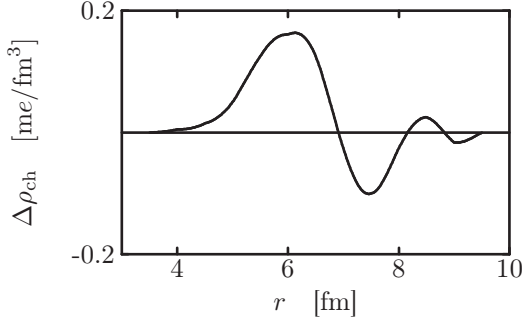
Fig. 3. Neutron charge contribution to the charge density distribution in ^{208}Pb. *me* stands for millielectron.

can be verified from the relation (9). Furthermore, in Ref. [9], where a different way has been used to include the effect of the neutron charge distribution, see previous section, the contribution to the radii has found to be small and a smooth function of N. This suggests that the result stated in relation (9) is model independent.
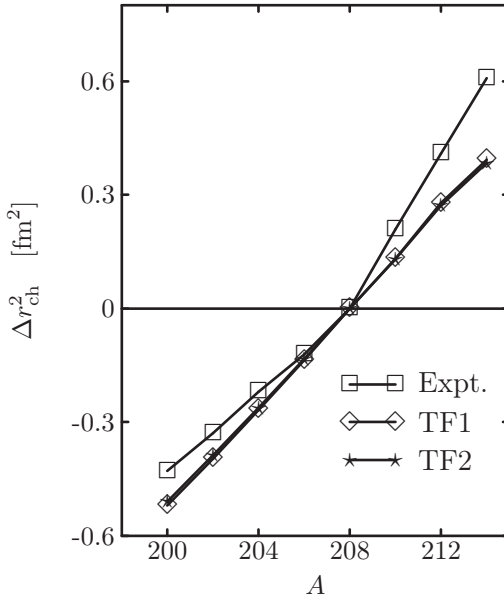

Fig. 4. Isotope shifts in the charge radii of Pb isotopes normalized to the nucleus ^{208}Pb as a function of the mass number A. TF1 and TF2 results are compared with the empirical data from Ref. [8]

Figure 4 shows the isotope shifts Δr_{ch}^2 of Pb-nuclei, which we calculate as:

$$\Delta r_{\text{ch}}^2(A) = \frac{1}{Z} \int d^3r \ r^2 \left(\rho_{\text{ch}} \left({}^A\text{Pb} \right) - \rho_{\text{ch}} \left({}^{208}\text{Pb} \right) \right) , \qquad (11)$$

since the computational calculation of this equation will produce much smaller numerical error (0.25%) than simply subtracting two r_{ch}^2 values from each other. The use of Eq. (3) instead of (1) changes the average slope, but as in Refs [4, 9] it does not give rise to a kink.

Comparing density distributions of neighboring isotopes is a common experimental practice, see Ref. [13]. Relative quantities are less sensitive to systematic errors and can be measured with greater accuracy than absolute measurements for a single nucleus. The experimental uncertainties in the isotope shifts in the charge radii of lead isotopes are comparable to the uncertainties in the experimental values of the radii themselves $(1-2\%)$ [13]. The uncertainties in the neutron skin thickness are large (25%) [13] due to the experimental uncertainty in the determination of the neutron rms radius. The deviations in the results of t are therefore not significant.

4. Conclusion

An analytical fit to the experimental data on the mean square charge radius of the neutron and to QCD-calculations of the neutron charge distribution is given and used to recognize the neutron charge distribution when calculating the charge density distribution in a finite nucleus. Charge density distributions in lead isotopes are calculated by utilizing the relativistic Thomas–Fermi approximation. The contribution from the charge distribution within the neutron changes the average slope of the Pb isotope shifts $\Delta r_{\text{ch}}^2(A)$, but does not give rise to a kink.

REFERENCES

[1] S. Kopecky, P. Riehs, J.A. Harvey,d N.W. Hill, *Phys. Rev. Lett.* **74**, 2427 (1995).

[2] Jo van den Brand, P. de Witt Huberts, *Physics World*, February 35, 1996.

[3] A. Bouyssy, J.F. Mathiot, N. Van Giai, *Phys. Rev.* **C36**, 380 (1987).

[4] N. Tajima, P. Bonche, H. Flocard, P.-H. Heenen, M.S. Weiss, *Nucl. Phys.* **A551**, 434 (1993).

[5] D. Von-Eiff, M.K. Weigel, Phys. Rev. **C46**, 1797 (1992).

[6] S. Haddad, M.K. Weigel, *Nucl. Phys.* **A578**, 471 (1994).

[7] M.M. Sharma, G. Lalazissis, P. Ring, *Phys. Lett.* **B317**, 3 (1993).

[8] M.M. Sharma, G. Lalazissis, J. König, P. Ring, *Phys. Rev. Lett.* **74**, 3744 (1995).

[9] W. Bertozzi, J. Friar, J. Heisenberg, J.W. Negele, *Phys. Lett.* **B41**, 408 (1972).

[10] B.D. Serot, J.D. Walecka, *Adv. Nucl. Phys.* **16**, 1 (1986).

[11] C.J. Horowitz, B.D. Serot, *Nucl. Phys.* **A368**, 503 (1981); **A399**, 529 (1983).

[12] A. Grasznahorskay, A. Balanda, J.A. Bordewijk, S. Brandenburg, M.N. Harakeh, N. Kalantar-Nayestanaki, B.M. Nyakó, J. Timár, A. van der Woude, *Nucl. Phys.* **A567**, 521 (1994).

[13] V.E. Starodubsky, N.M. Hintz, *Phys. Rev.* **C49**, 2118 (1994).